

Thermal Evolution of Neutron Stars in Two Dimensions

Rodrigo Negreiros* and Stefan Schramm

FIAS, Goethe University, Ruth Moufang Str. 1, 60438 Frankfurt, Germany

Fridolin Weber

*Department of Physics, San Diego State University,
5500 Campanile Drive, San Diego, California 92182, USA*

(Dated: June 5, 2022)

There are many factors that contribute to the breaking of the spherical symmetry of a neutron star. Most notably is rotation, magnetic fields, and/or accretion of matter from companion stars. All these phenomena influence the macroscopic structures of neutron stars, but also impact their microscopic compositions. The purpose of this paper is to investigate the cooling of rotationally deformed, two-dimensional (2D) neutron stars in the framework of general relativity theory, with the ultimate goal of better understand the impact of 2D effects on the thermal evolution of such objects. The equations that govern the thermal evolution of rotating neutron stars are presented in this paper. The cooling of neutron stars with different frequencies is computed self-consistently by combining a fully general relativistic 2D rotation code with a general relativistic 2D cooling code. We show that rotation can significantly influence the thermal evolution of rotating neutron stars. Among the major new aspects are the appearances of hot spots on the poles, and an increase of the thermal coupling times between the core and the crust of rotating neutron stars. We show that this increase is independent of the microscopic properties of the stellar core, but depends only on the frequency of the star.

PACS numbers: 04.40.Dg; 21.65.Cd; 26.60.-c; 97.60.Jd;

I. INTRODUCTION

The cooling of neutron stars has been used by many authors [1–22] as a way of probing the internal composition of these objects. Such studies rely on the fact that the physical quantities relevant for the cooling (specific heat, thermal conductivity, and neutrino emissions) strongly depend on the microscopic composition, so that different models lead to different thermal evolutions. For such studies, the predicted thermal evolution is compared to the observed data, with the ultimate goal of constraining the microscopic properties of neutron stars [4, 5]. An example of this is the recent analysis of the observed thermal behavior of the compact star in Cassiopeia A (Cas A) [10, 11, 23]. In these studies the authors link the observed thermal behavior of this neutron star to the onset of superfluidity in the stellar core. Possible alternative explanations have been suggested in [24, 25], where the observed data was explained in terms of the nuclear medium cooling scenario [24], and the a late onset of the Direct Urca process, triggered by the gravitational compression that accompanies a spinning-down neutron star [25].

In the standard approach, studies of the thermal evolution of neutron stars are performed by assuming that these stars are spherically symmetric. This assumption renders the thermal evolution calculations inherently one-dimensional (1D), which greatly simplifies the nu-

merical treatment. However, as pointed out by us in [25], rotation may play a very important role for the cooling of neutron stars. In [25] the effects of rotation on the microscopic composition, and its consequences for cooling, were studied. In the work presented here we investigate the macroscopic aspects of rotation on the cooling of neutron stars in the framework of a fully self-consistent two-dimensional (2D) treatment.

We shall consider the thermal evolution of rigidly rotating neutron stars. First we calculate the rotational structures of such stars, which is considerably more complicated than for spherically symmetric stars. The stellar structure is obtained by solving Einstein's field equation for a rotationally deformed 2D fluid [26, 27]. The numerical method used here is based on the KEH method [28–30]. The equation of state used for computing the global neutron star properties and its composition is a relativistic non-linear mean field (RMF) model, whose parameters are adjusted to the properties of nuclear matter at saturation density [31].

Once the structure of a rotating neutron star is computed, we solve the equations that govern the thermal evolution. The latter equations are re-derived for the metric of a 2D rotating neutron star. We show that the cooling of the object strongly depends on its frequency. At higher frequencies, rotating neutron stars show a substantial temperature difference between the equator and the pole. We also show that the time scale for the thermalization of such stars increases with its frequency.

This paper is organized as follows. In section II we discuss the energy balance and transport equations for a rotating neutron star. In section III we show the results for the surface temperature evolution of rotating neutron

*Electronic address: negreiros@fias.uni-frankfurt.de

stars. The internal temperature evolution is discussed in section IV. Finally, in section V we present our conclusions.

II. 2D THERMAL EVOLUTION

Given the complex nature of rotating neutron stars, where effects like frame dragging (Lense-Thirring effect) and additional self-consistency conditions (e.g. mass shedding, which sets an absolute limit on rapid rotation) are in place, carrying out a 2D study of the thermal evolution of such objects is a challenging task. First steps toward this direction were made in [25, 32–34]. We note that the cooling simulations performed in [34] are based on a standard spherically symmetric metric, since that study focused primarily on the impact of magnetic field effects on cooling. Differently from [34], we are presenting full 2D calculations of the thermal evolution of rotating neutron stars, taking into account the 2D metric of a rotating fluid distribution. The latter can be written as [26]

$$ds^2 = -e^{2\nu} dt^2 + e^{2\phi} (d\varphi - N^\varphi dt)^2 + e^{2\omega} (dr^2 + r^2 d\theta^2), \quad (1)$$

where $e^{2\phi} \equiv e^{2(\alpha+\beta)} r^2 \sin^2 \theta$ and $e^{2\omega} \equiv e^{2(\alpha-\beta)}$. The quantities ν , ϕ and ω denote metric functions, and N^φ accounts for the dragging of local inertial frames caused by the rotating fluid. All these quantities are functions of r and θ , and are implicitly dependent on N^φ . They need to be computed self-consistently from Einstein's field equation, $G^{\bar{\alpha}\bar{\beta}} = 8\pi T^{\bar{\alpha}\bar{\beta}}$, where $T^{\bar{\alpha}\bar{\beta}}$ denotes the fluid's energy momentum tensor.

The general relativistic equations of energy balance and transport are derived from the condition of energy-momentum conservation, and can be written as

$$\partial_r \tilde{H}_{\bar{r}} + \frac{1}{r} \partial_\theta \tilde{H}_{\bar{\theta}} = -r e^{\phi+2\omega} \left(\frac{1}{\Gamma} e^{2\nu} \epsilon + \Gamma C_V \partial_t \tilde{T} \right) - r \Gamma U e^{\nu+2\phi+\omega} \left(\partial_r \Omega + \frac{1}{r} \partial_\theta \Omega \right), \quad (2)$$

$$\partial_r \tilde{T} = -\frac{e^{\nu-\phi}}{r\kappa} \tilde{H}_{\bar{r}} - \Gamma^2 U e^{-\nu+\phi} \tilde{T} \partial_r \Omega, \quad (3)$$

$$\frac{1}{r} \partial_\theta \tilde{T} = -\frac{e^{\nu-\phi}}{r\kappa} \tilde{H}_{\bar{\theta}} - \Gamma^2 U e^{-\nu+\phi} \tilde{T} \frac{1}{r} \partial_\theta \Omega, \quad (4)$$

$$\Gamma U \partial_t \tilde{T} = -\frac{e^{-\omega-\phi}}{r\kappa} \tilde{H}_{\bar{\varphi}}, \quad (5)$$

where $\tilde{H}_i \equiv r e^{2\nu+\phi+\omega} H_i / \Gamma$, with H_i being the i -th component of the heat flux; $\tilde{T} \equiv e^\nu T / \Gamma$, with T being the temperature; κ is the thermal conductivity; C_V is the specific heat; ϵ is the neutrino emissivity; and the Lorentz factor $\Gamma \equiv (1 - U^2)^{-1/2}$, where U is the proper velocity with respect to a zero angular momentum observer, given by $U = (\Omega - N^\varphi) e^\phi$. In the case of rigid body rotation, which is considered here, one has $\Omega = \text{const}$ so

that Eqs. (2) to (5) reduce to

$$\partial_r \tilde{H}_{\bar{r}} + \frac{1}{r} \partial_\theta \tilde{H}_{\bar{\theta}} = -r e^{\phi+2(\alpha-\beta)} \left(\frac{e^{2\nu}}{\Gamma} \epsilon + \Gamma C_V \partial_t \tilde{T} \right), \quad (6)$$

$$\partial_r \tilde{T} = -\frac{1}{r\kappa} e^{-\nu-\phi} \tilde{H}_{\bar{r}}, \quad (7)$$

$$\frac{1}{r} \partial_\theta \tilde{T} = -\frac{1}{r\kappa} e^{-\nu-\phi} \tilde{H}_{\bar{\theta}}. \quad (8)$$

The standard cooling equations of spherically symmetric, non-rotating neutron stars are obtained from Eqs. (6) through (8) for $\Omega = 0$ and $\partial_\theta \tilde{T} = 0$ [26]. This work aims at solving Eqs. (6) to (8) for the temperature distribution $T(r, \theta; t)$ of non-spherical, rotating neutron stars. The boundary conditions are obtained by defining $\tilde{H}_{\bar{r}}$ at $r = 0$ and $R(\theta)$, and the heat flux $\tilde{H}_{\bar{\theta}}$ at $\theta = 0, \pi/2$ and at $r = R(\theta)$, with $R(\theta)$ denoting the stellar radius. The star's initial temperature, $T(r, \theta; t = 0)$, is typically chosen as $\tilde{T} \equiv 10^{11}$ K. Equations (3) and (4) can be solved for $\tilde{H}_{\bar{r}}$ and $\tilde{H}_{\bar{\theta}}$, differentiated with respect to r and θ , respectively, and then substituted into Eq. (2), which leads to the following parabolic differential equation (for $\nabla \Omega = 0$),

$$\partial_t \tilde{T} = -e^{\frac{2\nu}{r^2}} \frac{\epsilon}{C_V} + \frac{1}{r^2 \sin \theta} \frac{e^{3\nu-\gamma-2\xi}}{\Gamma} \frac{1}{C_V} \times \left(\partial_r \left(r^2 \kappa \sin \theta e^\gamma \left(\partial_r \tilde{T} \right) \right) + \frac{1}{r^2} \partial_\theta \left(r^2 \kappa \sin \theta e^\gamma \left(\partial_\theta \tilde{T} \right) \right) \right), \quad (9)$$

with the definitions $r \sin \theta e^{-\nu+\gamma} = e^\phi$ and $e^{-\nu+\xi} = e^{\alpha-\beta}$. Equation (9) is solved numerically in combination with a fully general relativistic rotation code, which provides the necessary macroscopic input quantities. The microscopic input quantities (e.g. specific heat, thermal conductivity, neutrino emissivity) are obtained from the chosen model for equation of state.

We should devote some time to discuss the microscopic model for the equation of state (EoS). In this work we used a non-linear relativistic mean-field model (parameter set G300) [31], which reproduces the properties of nuclear matter at saturation density. The underlying nuclear lagrangian has the form [26, 27, 31]

$$\begin{aligned} \mathcal{L} = & \sum_B \bar{\psi}_B [\gamma_\mu (i\partial^\mu - g_\omega \omega^\mu - g_\rho \vec{\rho}_\mu \vec{\psi} \gamma^\mu \vec{\tau}) - (m_N - g_\sigma \sigma)] \psi_B \\ & + \frac{1}{2} (\partial_\mu \sigma \partial^\mu \sigma - m_\sigma^2 \sigma^2) - \frac{1}{3} b_\sigma m_N (g_\sigma \sigma)^3 - \frac{1}{4} c_\sigma (g_\sigma \sigma)^4 \\ & - \frac{1}{4} \omega_{\mu\nu} \omega^{\mu\nu} + \frac{1}{2} m_\omega^2 \omega_\mu \omega^\mu + \frac{1}{2} m_\rho^2 \vec{\rho}_\mu \cdot \vec{\rho}^\mu - \frac{1}{4} \vec{\rho}_{\mu\nu} \cdot \vec{\rho}^{\mu\nu} \\ & + \sum_{\lambda=e^-, \mu^-} \bar{\psi}_\lambda (i\gamma_\mu \partial^\mu - m_\lambda) \psi_\lambda, \end{aligned} \quad (10)$$

where B stands for protons (p), neutrons (n), and hyperons (Σ, Λ, Ξ). The interactions among these particles are described via the exchange of σ , ρ , and ω mesons. Their masses are $m_\sigma = 550$ MeV, $m_\rho = 769$ MeV, and $m_\omega = 783$ MeV and their coupling constants are given

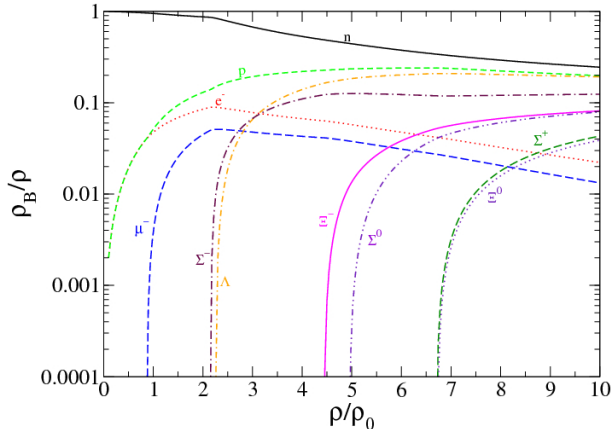


FIG. 1: (Color online) Particle composition obtained from Eq. (10). The quantity ρ denotes the baryon number density, ρ_0 is the number density at nuclear matter saturation density (0.16 fm^{-3}).

by $g_\sigma = 9.1373$, $g_\rho = 8.3029$, and $g_\omega = 8.6324$. The coupling constants of the self-interaction term of the σ meson are $b = 0.0033005$ and $c = 0.01529$ [27]. The particle population of neutron star matter computed from Eq. (10) is shown in Fig. 1.

The G300 EoS leads to a relatively high proton fraction, triggering the direct Urca process (DU hereafter) [35] in neutron stars with masses above $\sim 1.0 M_\odot$. As discussed in previous studies [3–11], the presence of the DU process enhances the cooling, leading to possible disagreement with observed data [4, 6]. This issue can be resolved by assuming that portions of the hadronic matter in the cores of neutron stars are in a superfluid state [3, 36, 37]. The presence of an enhanced cooling process allows us to track the heat propagation more clearly inside the rotating neutron star. This is due to the fact that, for rotating stars, the cold front originating from the stellar core is more intense (due to stronger neutrino emission, see [38]), and thus easier to track.

As for the neutrino emission processes taking place in the core, we have considered the direct as well as the modified Urca processes together with bremsstrahlung processes. A detailed review of the emissivities of such processes can be found in reference [39]. In addition to the core, we also consider the standard processes that take place in the crust of a neutron star [39]. The specific heat of the hadrons is given by the usual specific heat of fermions, as described in [4]. For the thermal conductivity we follow the calculations of [40].

III. SURFACE TEMPERATURE EVOLUTION

We now present the results for the thermal evolution of rotating neutron stars. We analyzed the thermal evo-

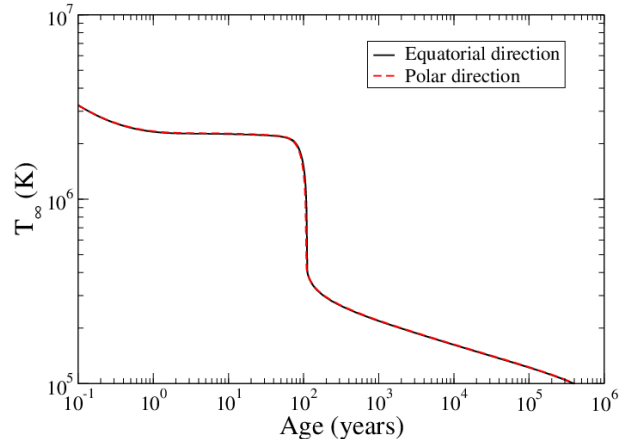


FIG. 2: (Color online) Redshifted temperature at star's pole and equator as a function of stellar age, for the 148 Hz star of table I.

lution of three different stellar configurations, each one with the same central density but rotating at different frequencies. The properties of these stars are listed in table I. Equation (9) was solved numerically for each star in

TABLE I: Properties of neutron stars whose thermal evolution is studied in this paper. All stars have a central density of 350 MeV/fm^3 . Their properties are computed for the relativistic mean-field EoS G300 [31]. M denotes the gravitational mass, R_e the equatorial radius, R_p the polar radius, $e = \sqrt{1 - (R_p/R_e)^2}$ the eccentricity, Ω the star's rotational frequency, and Ω_K is the mass shedding frequency.

M/M_\odot	R_e (km)	R_p (km)	e	Ω (Hz)	Ω_K (Hz)
1.28	13.25	13.11	0.14	148	1330
1.34	13.85	12.49	0.43	488	1275
1.48	15.21	11.50	0.65	755	1169

table I, and the results are shown in Figs. 2–4, where the redshifted temperatures at the poles and the equatorial belt of stars are plotted as a function of time.

In Figure 2 we show the cooling of a slowly rotating (148 Hz) neutron star. At such low frequencies there is no significant difference between the polar and equatorial temperature evolution, indicating that such stars cool essentially like spherically symmetric stars (the eccentricity of this star is just 0.14, as shown in table I). The situation is different for stars rotating at successively higher frequencies, as shown in Figs. 3 and 4. One sees that as the frequency increases, so does the difference between the polar and equatorial temperatures, with the pole being slightly warmer than the rest of the stellar surface due to the higher surface gravity there.

Another noticeable difference concerns the sharp temperature drop at ~ 100 years, which happens simul-

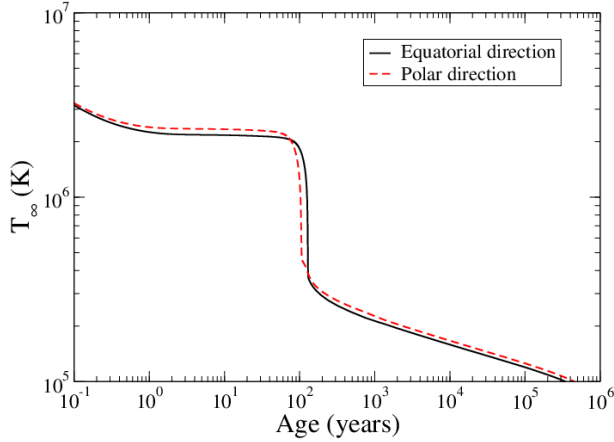


FIG. 3: (Color online) Same as Fig. 2, but for the 488 Hz star of table I.

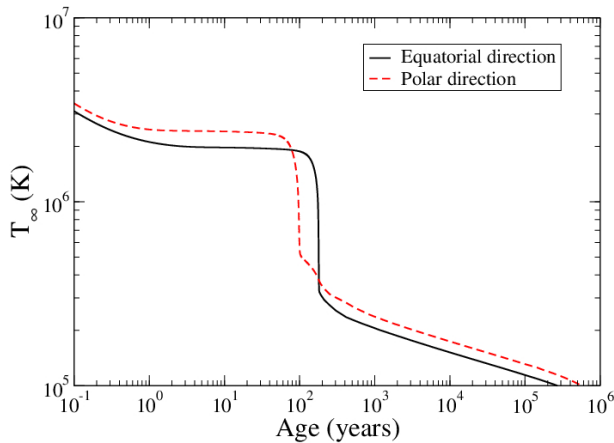


FIG. 4: (Color online) Same as Fig. 2, but for the 755 Hz star of table I.

taneously for the pole and equator of low frequency stars (i.e., spherical objects). This is not the case for stars rotating at higher frequencies, where a delay in the equatorial temperature drop is observed, as shown in Figs. 3 and 4. One can understand this sudden drop in surface temperature as the moment in time where the "cold front", spreading from the core to the surface, has reached the stellar surface. (From this moment on the interior of the star is in thermal equilibrium.) If fast neutrino processes, like the direct Urca process, are active in the core, the cold front will be more distinctive, leading to a more pronounced drop in temperature. The time at which the cold front reaches the surface depends strongly on the properties of the crust [38]. The cold front arrives first at the poles and then at the equator. This feature has its origin in the rotational deformation of the star: a flattening at

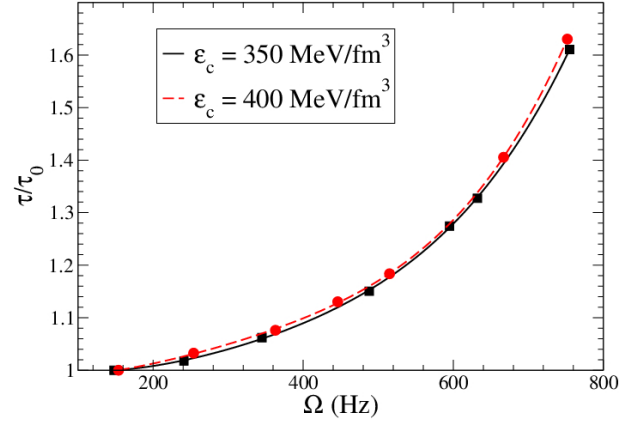


FIG. 5: (Color online) Dependence of core-crust thermal coupling time, τ , on rotational frequency of a neutron star. The quantity ϵ_c denotes the star's central density. Solid dots show the outcome of our numerical calculations, the lines show a 4th order polynomial fit to the data.

the pole (leading to a thinner crust in this region) and an expansion at the equator (leading to a thicker crust). The thinner crust in the polar region, combined with the lower fluid velocity, leads to a more efficient heat propagation, allowing the cold front to reach the pole more quickly, as shown in Figs. 3 and 4. This effect is less distinctive for stars with lower frequencies, since their shapes tend to be spherically symmetric and their crusts are more uniform.

Keeping in mind that the core-crust thermal coupling time (τ) depends primarily on the crust properties, and that the macroscopic properties of the crust are directly connected to the stellar rotation rate, we now investigate the dependence of τ on the frequency of the star. In order to do that we calculate the cooling of two sets of stars, each set having central densities of 350 and 400 MeV/fm³, and covering the range of frequencies from 100 and 800 Hz. For each star we calculate τ/τ_0 , with τ_0 being the core-crust coupling time in the spherically symmetric case (i.e. $\Omega = 0$), and τ the corresponding value for rotating neutron stars (defined as the moment that the cold front reaches the equator). The results are shown in Fig. 5. We find that τ/τ_0 can be fitted well by a 4th order polynomial, and that the result is independent of the microscopic properties of the core, as can be seen in Fig. 5. The indication is that this result should hold regardless of the EoS used for the core, as long as the crustal composition is the same.

IV. INTERIOR TEMPERATURE EVOLUTION

In order to better understand the thermal evolution of a rotating star, we now analyze the interior temperature

evolution of such objects. The star rotating at $\Omega = 755$ Hz will be used for this analysis, since its strong deformation allows us to better evaluate the effects of rotation on cooling. The results of this analysis can be generalized to stars rotating at lower frequencies.

Figure 6 shows a series of snapshots of the temperature profiles of the $\Omega = 755$ Hz star. Displayed are different cooling stages of this neutron star. For an early age of 0.1 year (Fig. 6 (a)) the core and crust are thermally decoupled, which can be clearly seen by the much higher temperature of the crust. Also clearly noticeable is the higher temperature of the pole, which is due to the greater surface gravity in this region. Fig. 6 (a) also shows that the core is much colder than the outer layers, which is a consequence of the fast core cooling via the DU process. The cold interior region will propagate like a “cold front” until it finally reaches the surface, at which point the star has become thermalized. The propagation of the cold front can be observed in Fig. 6 (b), which shows the temperature profile at a stellar age of 40 years. As already mentioned in section III, the cold front propagates more efficiently in the polar direction, allowing this region to couple with the core more quickly than the equatorial regime (see also Figs. 2 to 4). Figure 6 (c), (d) and (e) illustrate stellar epochs where the cold front is reaching the surface, first the polar region (Fig. 6 (c)), and then propagating downward towards the equatorial region (Fig. 6 (d) and (e)). After 190 years, the stellar interior has reached thermal equilibrium, as shown in Fig. 6 (f). For ages greater than 190 years the pole is warmer than the equator, as was the case for Figs. 6 (a) and (b). The temperature difference is too small, however, to be noticeable in Fig. 6 (f).

The surface temperatures shown in Fig. 6 are the redshifted surface temperatures. This temperature is a function of the mantle’s temperature (more specifically of the last layer of the crust) [41, 42].

V. DISCUSSION AND CONCLUSIONS

The objective of this work was to investigate in detail the cooling of rotationally deformed neutron stars in 2 dimensions (2D). Our investigation is fully self-consistent. Einstein’s field equations of rotating compact objects have been solved in combination with a 2D cooling code. Such studies are extremely important if one wants to understand the thermal evolution of stellar systems where spherical symmetry is broken. This might be the case for highly magnetized neutron stars, neutron stars that are spinning down from high to low rotation rates, as well as for accreting neutron stars which are being spun up to high rotation rates. This work represents the first step towards a widely applicable, fully self-consistent treatment of the cooling of neutron stars whose spherical symmetries have been broken. As a first

step in this direction, we considered here rigidly rotating, rotationally deformed neutron stars. The metric of such objects is significantly different from the metric of spherically symmetric stars; we therefore re-derived the general relativistic equations that govern the thermal evolution of such stars.

The microscopic model for the equation of state (EoS) which was used in our study is that of purely hadronic matter, with the whole baryon octet included. This model for the EoS allows for the direct Urca process in stars with masses above $1.0 M_{\odot}$, which leads to enhanced stellar cooling. This choice for the equation of state was intentional, since the direct Urca process yields sharper temperature gradients inside the star, which allow us to track the energy transport more clearly. After obtaining a solid understanding of the thermal evolution of rotating compact stars, our study will be applied in a future study to compact objects with more complex core compositions, such as hadronic superfluids, boson condensates, or quark matter.

Our results indicate that rotation (and hence the 2D structure) plays an important role for the thermal evolution of neutron stars. The most important features can be summarized as follows:

- The redshifted temperature of the pole is slightly higher than the temperature at the equator, which is due to the difference in surface gravity between these two regions.
- Thermal energy is more efficiently transported along the polar direction, due to the lower fluid velocities and thinner crust there. This allows a “cold front”, originating from the core, to arrive at the pole sooner than at the equator.

With respect to the second item above, we have found that the increase in the core-crust coupling time is independent of all stellar properties, except the frequency. This is consistent with the fact that the crusts of the neutron star at different rotational stages are very similar regardless of their core composition, and that the only factor (in the present study) that alters the macroscopic properties of the crust is rotation. This is indicated by the increase in the core-crust coupling time as a function of frequency, which is very similar for objects with different central densities (and thus different particle compositions).

Acknowledgement. F.W. is supported by the National Science Foundation (USA) under Grant PHY-0854699. R.N. and S.S. acknowledge access to the computer facilities of the CSC Frankfurt. R.N. acknowledges financial support from the LOEWE program HIC for FAIR.

-
- [1] S. Tsuruta and A. G. W. Cameron, *Nature* **207**, 364 (1965).
 - [2] O. V. Maxwell, *The Astrophysical Journal* **231**, 201 (1979).
 - [3] C. Schaab, F. Weber, M. Weigel, and N. K. Glendenning, *Nuclear Phys A* **605**, 531 (1996).
 - [4] D. Page, J. Lattimer, M. Prakash, and A. W. Steiner, *The Astrophysical Journal Supplement Series* **155**, 623 (2004).
 - [5] D. Page, U. Geppert, and F. Weber, *Nuclear Physics A* **777**, 497 (2006).
 - [6] D. Page, J. Lattimer, M. Prakash, and A. W. Steiner, *The Astrophysical Journal* **707**, 1131 (2009).
 - [7] D. Blaschke, T. Klähn, and D. Voskresensky, *The Astrophysical Journal* **533**, 406412 (2000).
 - [8] H. Grigorian, D. Blaschke, and D. Voskresensky, *Physical Review C* **71**, 1 (2005).
 - [9] D. Blaschke, D. Voskresensky, and H. Grigorian, *Nuclear Physics A* **774**, 815 (2006).
 - [10] D. Page, M. Prakash, J. Lattimer, and A. Steiner, *Physical Review Letters* **106**, 081101 (2011).
 - [11] D. G. Yakovlev, W. C. G. Ho, P. S. Shternin, C. O. Heinke, and A. Y. Potekhin, *Monthly Notices of the Royal Astronomical Society* **411**, 1977 (2011).
 - [12] C. Schaab, D. Voskresensky, A. Sedrakian, and F. Astronomy and Astrophysics **604**, 591 (1997).
 - [13] P. S. Shternin, D. G. Yakovlev, C. O. Heinke, W. C. G. Ho, and D. J. Patnaude, *Monthly Notices of the Royal Astronomical Society: Letters* **412**, L108 (2011).
 - [14] I. Shovkovy and P. Ellis, *Physical Review C* **66**, 1 (2002).
 - [15] M. Prakash, J. Lattimer, and C. Pethick, *Astrophysical Journal* **390**, L77 (1992).
 - [16] J. M. Lattimer, K. A. van Riper, M. Prakash, and M. Prakash, *The Astrophysical Journal* **425**, 802 (1994).
 - [17] M. E. Gusakov, A. D. Kaminker, D. G. Yakovlev, and O. Y. Gnedin, *Monthly Notices of the Royal Astronomical Society* **363**, 555 (2005).
 - [18] J. Horvath, O. Benvenuto, and H. Vucetich, *Physical Review D* **44**, 3797 (1991).
 - [19] F. Weber, R. Negreiros, and P. Rosenfield, *Astrophysics and Space Science Library* **357**, 213 (2009).
 - [20] R. Negreiros, V. A. Dexheimer, and S. Schramm, *Physical Review C* **82**, 1 (2010).
 - [21] B. Niebergal, R. Ouyed, R. Negreiros, and F. Weber, *Physical Review D* **81**, 1 (2010).
 - [22] M. Alford, P. Jotwani, C. Kouvaris, J. Kundu, and K. Rajagopal, *Physical Review D* **71**, 1 (2005).
 - [23] C. O. Heinke and W. C. G. Ho, *The Astrophysical Journal* **719**, L167 (2010).
 - [24] D. Blaschke, H. Grigorian, D. N. Voskresensky, and F. Weber, [arXiv:1108.4125v1](https://arxiv.org/abs/1108.4125v1) [nucl-th].
 - [25] R. Negreiros, S. Schramm, and F. Weber, [arXiv:1103.3870v4](https://arxiv.org/abs/1103.3870v4) [astro-ph.HE].
 - [26] F. Weber, *Pulsars as astrophysical laboratories for nuclear and particle physics* (Institute of Physics, Bristol, 1999), 1st ed.
 - [27] N. K. Glendenning, *Compact stars: nuclear physics, particle physics, and general relativity* (Springer, 2000), 1st ed.
 - [28] H. Komatsu, Y. Eriguchi, and I. Hachisu, *Royal Astronomical Society, Monthly Notices* **237** (1989).
 - [29] G. B. Cook, S. L. Shapiro, and S. A. Teukolsky, *The Astrophysical Journal* **398**, 203 (1992).
 - [30] N. Stergioulas and J. L. Friedman, *The Astrophysical Journal* **444**, 306 (1995).
 - [31] N. K. Glendenning, *Nuclear Physics A* **493**, 521 (1989).
 - [32] C. Schaab and M. K. Weigel, *Astron. & Astrophys.* **336**, L13 (1998).
 - [33] M. Stejner, F. Weber, and J. Madsen, *The Astrophysical Journal* **694**, 1019 (2009).
 - [34] J. A. Pons, J. A. Miralles, and U. Geppert, *Astronomy and Astrophysics* **496**, 207 (2009).
 - [35] J. Lattimer, C. Pethick, M. Prakash, and P. Haensel, *Physical review letters* **66**, 27012704 (1991).
 - [36] K. P. Levenfish and D. G. Yakovlev, *Astronomy Letters* **20**, 43 (1994).
 - [37] D. Page, M. Prakash, J. M. Lattimer, and A. W. Steiner, p. 28 (2011).
 - [38] O. Y. Gnedin, D. G. Yakovlev, and A. Y. Potekhin, *Monthly Notices of the Royal Astronomical Society* **324**, 725 (2001).
 - [39] D. G. Yakovlev, A. D. Kaminker, O. Y. Gnedin, and P. Haensel, *Physics Reports* **354**, 1 (2001).
 - [40] E. Flowers and N. Itoh, *The Astrophysical Journal* **250**, 750 (1981).
 - [41] E. H. Gudmundsson, C. J. Pethick, and R. I. Epstein, *The Astrophysical Journal* **272**, 286 (1983).
 - [42] A. Y. Potekhin, G. Chabrier, and D. G. Yakovlev, *Astronomy and Astrophysics* **323**, 415 (1997).

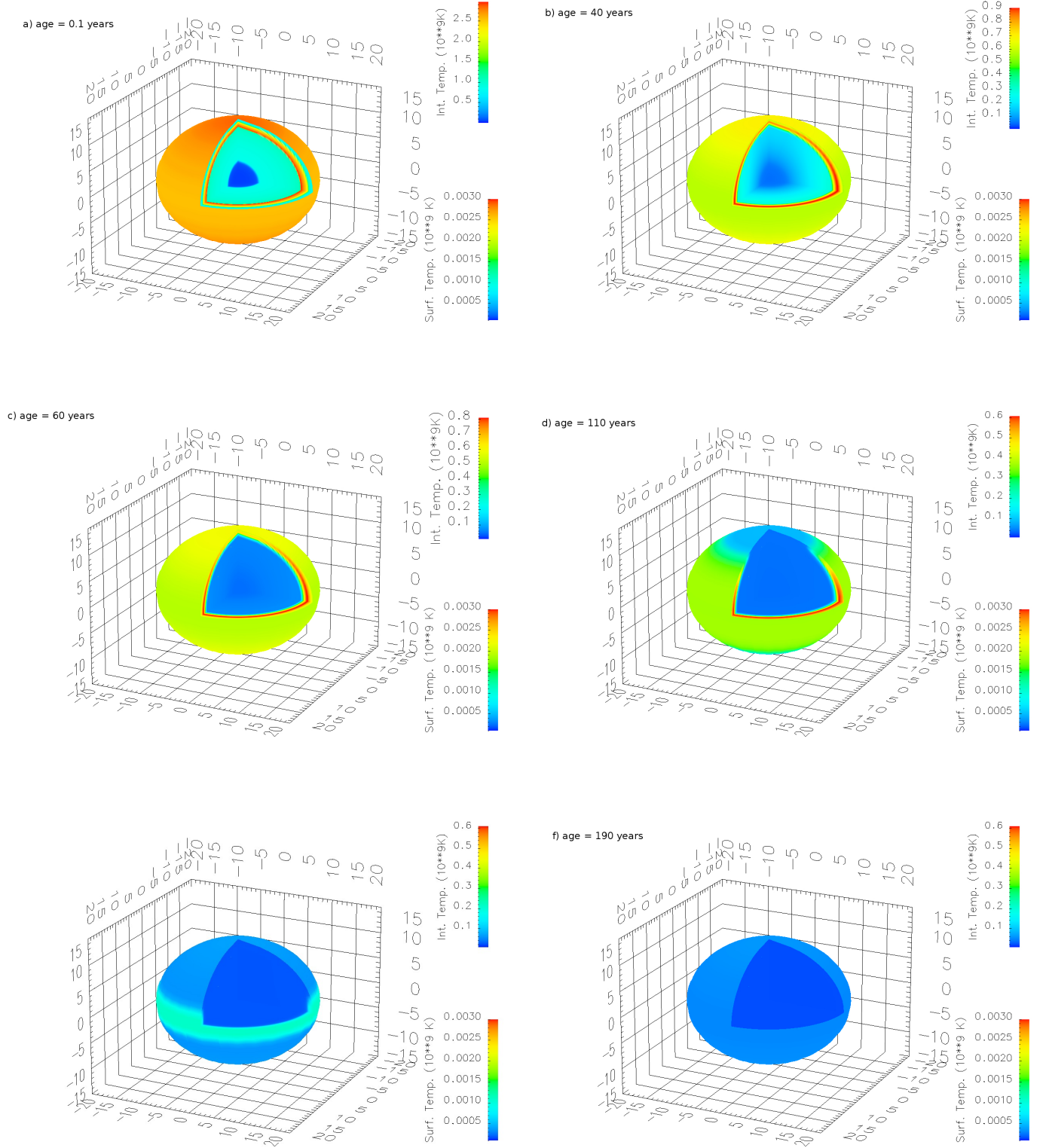


FIG. 6: (Color online) Temperature profiles of a neutron star rotating at $\Omega = 755$ Hz at different stages of stellar evolution, ranging from 0.1 (a), 40 (b), 60 (c), 110 (d), 170 (e), to 190 (f) years. The colors represent the redshifted temperature. The stars are cut open to help visualize the interior temperature evolutions.